Predictive Centroiding for Single and Multiple FOVs Star Trackers[1]

Malak A. Samaan[2], Daniele Mortari[3], Thomas C. Pollock[4], and John L. Junkins[5]

Department of Aerospace Engineering,
Texas A&M University, College Station, TX 77843-3141

ABSTRACT

Star centroiding, locating the star image center in a CCD image, is a fundamental process for any star tracker. In this paper, the approximate location of the stars in successive image frames are predicted using the angular velocity as provided by the rate gyro, then the centroid is updated based upon local image processing. When the rate gyro data are not available, then the angular velocity is estimated using kinematics equation and successive attitude estimates from the Lost-In-Space Algorithm. Also of interest are the special features of non-circular star image shapes associated with optical tagging of starlight and/or image smear. And finally, an approach is presented to implement these ideas with recently introduced Active Pixel Sensors, allowing dynamic pixel access and selected subarray analog-to-digital conversion of the pixel information is feasible, with logic dictated by most recent image and the instantaneous angular velocity estimate. The resulting process predicts the CCD starlight locations and thus, we call the resulting algorithm *predictive centroiding*. The problem of the image smear is also treated, in which the relatively high angular velocity of the Spacecraft will affect the shape of the star images.

[1]Paper AAS 02-103 presented at the AAS/AIAA Space Flight Mechanics Meeting, San Antonio, TX, 27-31 January, 2002.

[2]Graduate Student, 722 Bright Bldg., Department of Aerospace Engineering, Texas A&M University, College Station, TX 77843-3141, mas1894@aero.tamu.edu

[3]Assistant Professor, Università degli Studi "La Sapienza" di Roma, Via Salaria, 851 - 00138 Roma, Italy. Tel/Fax: +39 (06) 88346-432, mortari@psm.uniroma1.it

[4]Associate Professor, Department of Aerospace Engineering, Texas A&M University, College Station, TX 77843-3141, Tel: (979) 845-1686, Fax: (979) 845-6051, pollock@tamu.edu

[5]George J. Eppright Chair Professor, Director of the Center for Mechanics and Control, 722 Bright Bldg., Department of Aerospace Engineering, Texas A&M University, College Station, TX 77843-3141, Tel: (979) 845-3912, Fax: (979) 845-6051, junkins@tamu.edu

Introduction

Star trackers are widely used in spacecraft attitude determination because they produce higher accuracy attitude estimates than any other existing sensors. In order to maximize the accuracy of the star direction estimation, the starlight is usually de-focused over 3×3 to 15×15 pixel array masks, depending on the sensor CCD design and/or on the star magnitude. The resulting shape of the CCD starlight spot is usually described by Point Spread Functions (PSFs) which are near-Gaussian. The appropriate optical designs defocus the starlight and utilizing modern image centroiding techniques allows estimating the star direction with a precision of about 1/10 of a pixel or better.

The image centroiding is, therefore, a fundamental process to increase the attitude data set accuracy. Recently, with the introduction of multiple field of view star trackers [1] (which output non-circular images to identify the associated field of view), the centroiding algorithms have new challenges to meet. The speed and accuracy to accomplish the centroiding process represent, therefore, the units of measure to compare the existing different approaches. The fact that the frame rate of star trackers using an advanced Active Pixel Sensor can be relatively high (10 to 100 Hz), and for small optics and associated realistic integration times, the maximum angular velocity will necessarily be fairly low (significantly less than one degree/sec). In view of these considerations, a typical star will be imaged many successive times (typically, several hundred times) before it leaves the field of view. In successive image processing, to enable local access and analog-to-digital conversion of only those pixels where starlight is likely to be found, we can make use of previous star locations and the approximately linear displacement of the star locations from one frame to another one.

In many applications, we can simply assume $\omega\delta t$ is the differential angular displacement of the star sensor and map this rotation into linearly predicted displacements of the image centers for all stars, where ω is the angular velocity vector and δt is the time interval between successive frames. This linear approximation is usually more than adequate to center the starting adaptive mask for computing star centroids, since the small errors in the starting approximation for centering the mask simply accelerate the process of finding the data to centroid; using the approach we present herein, there is negligible effect on the final centroid approximation. The predictive centroiding algorithm is implemented to be used in the GIFTS EO-3 (Geostationary Imaging

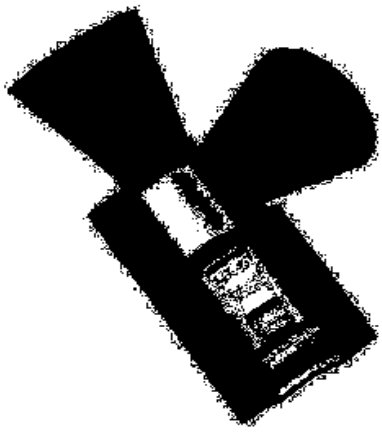

Figure 1: StarNav II Split Field of View Star Camera

Fourier Transform Spectrometer) mission. Figure 1 provides a schematic of the split FOV camera that will be used in the GIFTS mission. The electro-optical details of this camera design are the subject of a pending patent (Ref [2]).

Predictive Centroiding Steps

Once we have the star image, taken by one or multiple FOVs camera, the centroiding process is needed. Initially, the image will be treated using the usual centroiding techniques which use the mass moment method to find the location of the star in the image. This is the most common approach and has been motivated by the acquisition and tracking algorithms developed historically for the ASTROS star tracker developed at NASA JPL [3]. After the first image, the following images will be processed using our new technique, *predictive centroiding*. Predictive centroiding will be treated for the one, two and three Field Of View (FOV) star trackers [1, 4, 5]. The steps of predictive centroiding are stated as follows:

1. The attitude matrix (projecting body frame directions onto the inertial frame), $C(t_0)$ evaluated at initial time, is calculated using the Lost In Space Algorithm (LISA) [9].

2. Using the initial angular velocity data, we can predict the attitude matrix at the current frame $C_p(t+\delta t)$ using the previous attitude matrix

$C(t)$, and the following linear approximation

$$C_p(t+\delta t) = [I - \tilde{\omega}\delta t]C(t) \tag{1}$$

where $\tilde{\omega}$ is the cross product matrix populated with the components of the angular velocity vector ω. For virtually all current anticipated missions, $\|\tilde{\omega}\delta t\| < 10^{-3}$ rad., so Eq. (1) should be accurate to micro radian or better precision for one time step prediction.

3. The vectors associated with the four corners of the FOV are projected to the inertial reference frame using the predicted attitude matrix.

4. By accessing the star catalog using a bounding box whose vertices are the sensor four corners, we can access the inertial reference vectors $\hat{\mathbf{v}}_i$ to stars imaged in that frame.

5. Given the attitude matrix $C^{\mathrm{T}}(t) \equiv [\,\hat{\mathbf{c}}_1 \quad \hat{\mathbf{c}}_2 \quad \hat{\mathbf{c}}_3\,]$ at time t, and the inertial star vectors $\hat{\mathbf{v}}_i$, $(i = 1, \ldots, n)$, the star locations (x_i, y_i) are evaluated by the co-linearity equations:

$$x_i = x_0 - f\,\frac{\hat{\mathbf{c}}_1^{\mathrm{T}}\hat{\mathbf{v}}_i}{\hat{\mathbf{c}}_3^{\mathrm{T}}\hat{\mathbf{v}}_i} \qquad \text{and} \qquad y_i = y_0 - f\,\frac{\hat{\mathbf{c}}_2^{\mathrm{T}}\hat{\mathbf{v}}_i}{\hat{\mathbf{c}}_3^{\mathrm{T}}\hat{\mathbf{v}}_i} \tag{2}$$

where f is the camera focal length and x_0, y_0 are the optical axis offsets.

6. For the considered frame, once the star locations are predicted, then these locations become the center of masks used for centroiding for the real CCD image.

7. The recursive star identification algorithm [6], which uses the star neighbor approach, will then be used to identify the observed stars for that frame. The optimal estimate of the attitude matrix $C(t+\delta t)$ will be determined by using the ESOQ-2 method [7], and the associated angular velocity estimate will be calculated from kinematics equation $\dfrac{dC}{dt} = -\tilde{\omega}\, C$, by replacing differentials with small finite differences

$$\tilde{\omega} = \left[I - C(t+\delta t)\, C^{\mathrm{T}}(t)\right]/(\delta t) \tag{3}$$

8. The best estimate of angular velocity will be used to determine the predicted star locations at next frame and the loop will start again from step 2.

Some simulation results are shown in Figs. 2 and 3, for one FOV camera where two sequential images are superimposed and the two sets of star locations are shown to indicate the image motion. Also, for the case of two superimposed orthogonal FOVs of a split field of view camera (StarNav II), the Figs. 4 and 5 show the star images and the star locations for two adjacent in time images. Figures 2 and 4 have been obtained using the recently developed "Virtual CCD" software (Ref. [4, 5]).

In Fig. 4, the elliptical star images associated with the "Optical tagging method" for denoting which FOV the stars were imaged, are shown. Notice that astigmatism distortion is deliberately introduced (Ref. [2]) to cause the normally circular PSF to become elliptical. The eigenvalue of the figure inertia tensor associated with the "stretched" direction (eigenvector), indicates the FOV of origin for each star image. For example, in Fig. 4, the vertically stretched elliptical images are from the left FOV, whereas the horizontally stretched images are from the right FOV. Obviously, the shape of the images can easily be detected during image processing by using the eigenvalue ratio between the inertia principal axes of the mask surrounding each non-circular star image. These results also show that the time required to find the centroids using predictive centroiding is less by one order of magnitude than the time required using the regular centroiding techniques. From a mathematical point of view, if $[x_c, y_c]$ are the coordinates of the centroiding, then

$$J_1 = \sum_i (y_i - y_c)^2 \qquad \text{and} \qquad J_2 = \sum_i (x_i - x_c)^2 \tag{4}$$

are the principal figure MOI, where the sums are extended to all of the pixels (coordinate $[x_i, y_i]$) used for centroiding. Therefore, the FOV identification is simply dictated by

$$J_1 < J_2 \qquad \text{or} \qquad J_1 > J_2 \tag{5}$$

provided that $(J_1 - J_2)^2$ is greater than a given numerical threshold.

The number of pixels processed is reduced from $512 \cdot 512 = 262,144$ to approximately $(n \cdot m)$, where n is the number of stars and m is the number of pixels associated with the average star images. For a typical images, $n \cdot m \simeq 8 \cdot 25 \simeq 200$, so four order of magnitude less image data is involved; this suggest that further algorithm optimization may greatly improve over the one order of magnitude advantage gained.

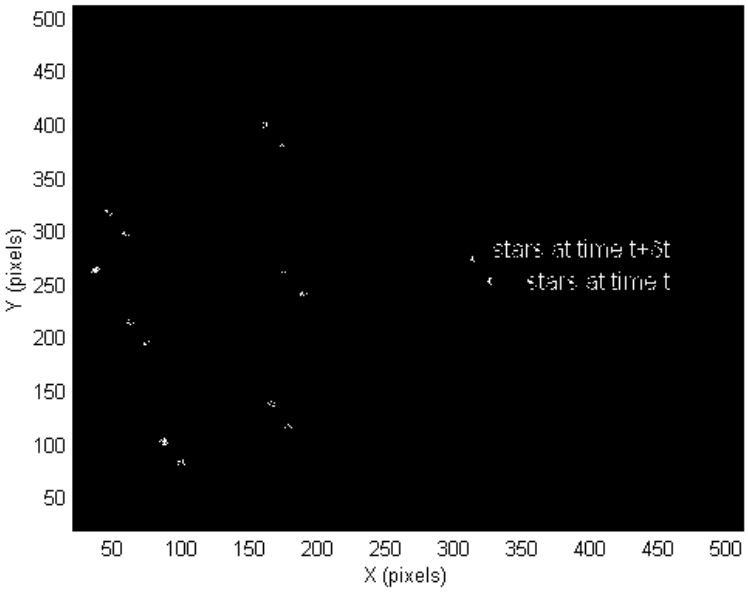

Figure 2: Two Superimposed Images for One FOV

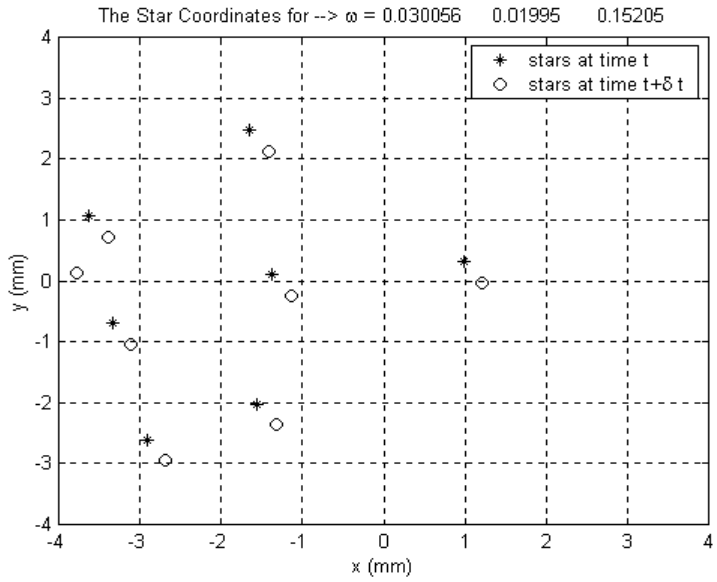

Figure 3: Single FOV Image Centroid Locations

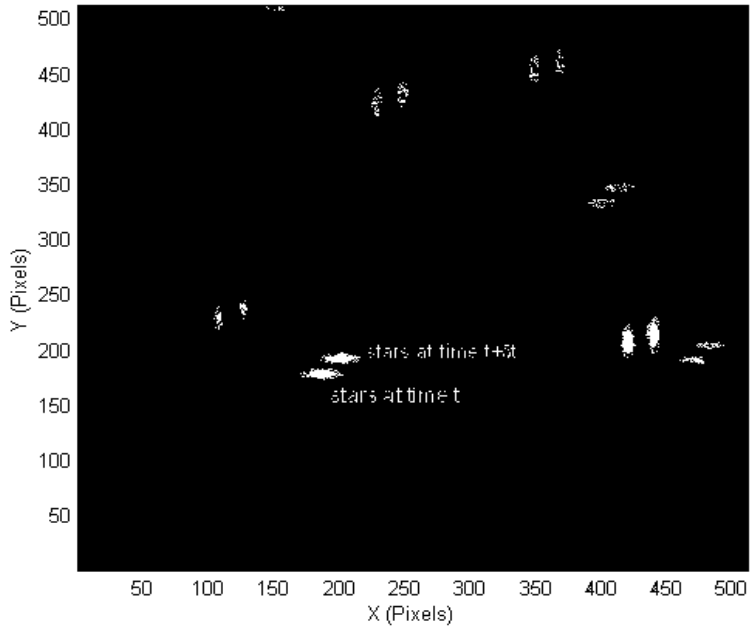

Figure 4: Two Superimposed Images for Two FOVs

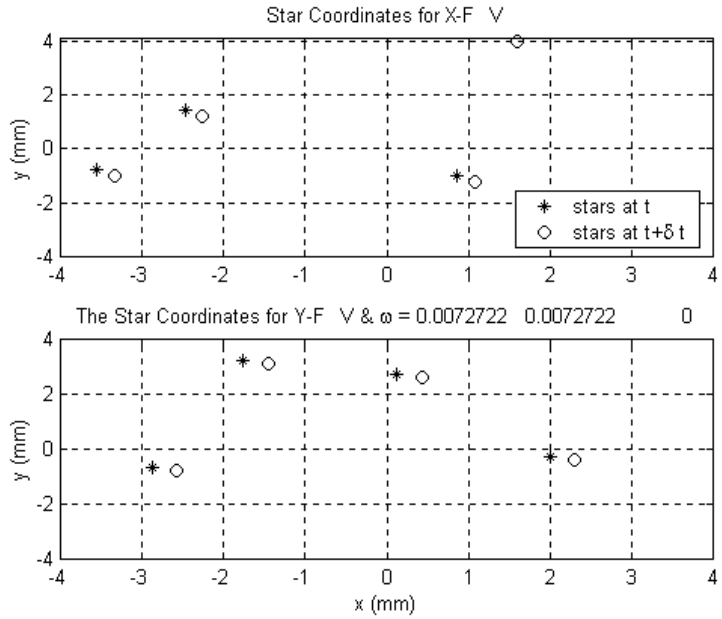

Figure 5: Two FOV Image Centroid Locations for the Pair of Images

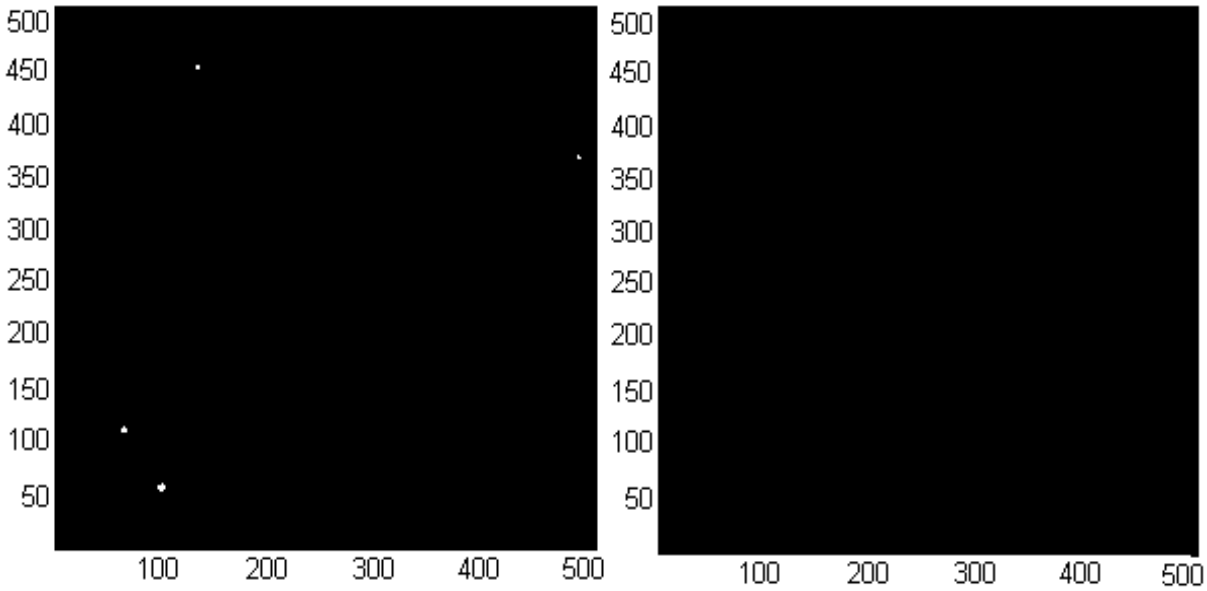

Figure 6: Star image W/O Smear (left), and Star image with Smear (right)

The Effect of Image Smear

The image smear is taking place in the focal plane of the imaged stars for slow values of the integration time t_s, or for high values of the S/C angular velocity ω. Figure 6 shows a simulated star image for a randomly oriented star tracker. The StarNav I camera having 512×512 pixels and 58 mm focal length, is used to perform these simulations, night sky images are planned to validate these results when the prototype design is completed in spring 2002. The left figure of Fig.6 shows the stars without image smear and the right one shows the same image with image smear for $\omega = 0.2$ deg/sec and for $t_s = 30$ msec. These simulated images are created using the fact that the volume of the intensity of each star will be constant during the integration time while the star area will increase with increasing the smear. We note that implementing the split field of view, with astigmatism tagging, presents a difficulty if there is significant image smear, because it will be difficult to distinguish between smear and astigmatism. As a consequence, the astigmatism idea will restrict the angular velocity to be below a thresh-hold value with negligible image smear.

t_s (msec)	10	20	30	50
$\omega_{\max}$ (deg/sec)	0.156	0.078	0.052	0.0313

Table 1: Maximum angular velocity

Maximum Angular Rate Estimation

The centroiding techniques allow the star direction with a precision of 1/10 of a pixel or better; this conservative estimate is derived from night sky experiments. From Fig. (7) we can calculate the corresponding maximum

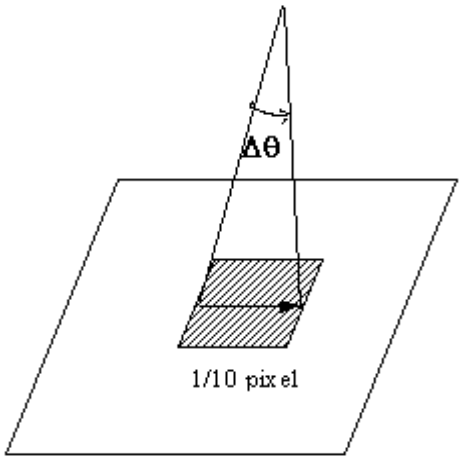

Figure 7: Centroiding Accuracy

allowed separation angle for totally negligible image smear as $\Delta\vartheta = 1/10$ (chip size/number of pixels). The critical condition $\Delta\vartheta = \omega\delta t$, where δt is the integration time and ω is the angular rate of the spacecraft corresponds to image smear $\Delta\vartheta$ being equal to the random, approximately Gaussian centroiding errors. The analytical values of the maximum angular velocity, for negligible image smear as a function of integration time are calculated for 512×512 CCD camera and a 7^o field of view. Table (1) summarizes the results of the analytical value of the maximum angular for each integration time.

For $\omega < \omega_{max} = \Delta\vartheta/\delta t$ results in negligible image smear, however, we find in practice that acceptable centroid accuracy may be obtained, for perhaps

3 or 4 times this "max" angular velocity, which will be discussed in the next section.

Measurement Errors and the Standard Deviation Computation

For the star images, taken with smear effect, the attitude associated with the image should be most valid at $(t + \delta t/2)$. So, if no smear the $\Delta\vartheta = \omega\delta t$ is negligible and the attitude matrix is $C(t)$. For the smear case the attitude matrix at $(t + \delta t/2)$ is

$$C(t + \delta t/2) = [I - \tilde{\omega}\delta t/2]\, C(t) \tag{6}$$

The equivalent angular centroiding (measurement) error is estimated from a finite sample (N) as

$$\sigma^2 = \frac{1}{N} \sum_{i=1}^{n-1} \sum_{j=i+1}^{n} (\vartheta_{ij}^M - \vartheta_{ij}^C)^2 \tag{7}$$

where ϑ_{ij}^M is the interstar angle measured from smeared image, ϑ_{ij}^C is the corresponding interstar angle from cataloged vectors, $N = n(n-1)/2$ is the number of star pairs, and n is number of measured stars. Also, the standard deviation for the centroiding errors can be calculating from rectangular image coordinates as

$$\text{STD} = \frac{1}{f} \sqrt{\text{STD}(x^M - x^C)^2 + \text{STD}(y^M - y^C)^2} \tag{8}$$

The above simulations for the star images with and without smear are used to calculate the measurement error and the STDs, for different angular velocities and integration times. Notice σ^2 can be computed from measured and cataloged interstar angles without using an attitude estimated, whereas STD depends upon predicted image plane coordinates (x^C and y^C); these can only be computed using the best attitude estimate. While both σ^2 and STD are meaningful, σ^2 is not "corrupted" by attitude estimation errors and is therefore considered better measure.

Table (2) shows the effect of smear on the centroiding errors for integration times equal to 10, 20, and 30 msec, respectively. This table is created using a finite number of samples (a hundred star images is used), but is believed converged to within 1% or better. A large number of actual night sky

$t_s = 10$ msec	ω (deg/sec)	0.01	0.02	0.05	0.10	0.20	0.25	0.30
$t_s = 10$ msec	$\sigma_{w/o}$ (μ rad)	35.6	-	-	-	-	-	35.6
$t_s = 10$ msec	σ_{smear}	36.0	36.5	36.7	37.5	56.4	60.6	105.0
$t_s = 10$ msec	$\text{STD}_{w/o}$	39.1	-	-	-	-	-	39.1
$t_s = 10$ msec	STD_{smear}	39.1	39.2	39.6	41.2	51.7	57.0	97.0
$t_s = 20$ msec	ω	0.01	0.02	0.05	0.10	0.15	0.20	0.25
$t_s = 20$ msec	σ_{smear}	35.6	35.9	37.4	56.8	168.0	246.0	429.0
$t_s = 20$ msec	STD_{smear}	39.7	42.0	44.6	52.4	54.4	228.0	424.0
$t_s = 30$ msec	ω	0.01	0.02	0.05	0.10	0.15	0.20	0.25
$t_s = 30$ msec	σ_{smear}	37.0	38.2	45.5	81.9	292.4	521.0	808.2
$t_s = 30$ msec	STD_{smear}	39.5	42.8	47.7	76.0	284.8	485.8	773.0

Table 2: Measurement Errors and Standard Deviations for Various Cases

images would be required to validate the numbers given in Table (2). Notice that accuracy degrades slowly with ω, until $\omega \cong 2.\omega_{max}$, see table (1).

As expected the measurement errors and the standard deviation estimates get worse with increasing smear. So, by comparing Table (1) with Table (2) we can conclude that, the actual angular velocity can be increased by factor of about two to three from the analytical maximum angular velocity estimate in Table (1), with small to moderate accuracy degradation.

Conclusion

This paper presents predictive centroiding as a new approach for fast image processing for the star trackers. It enables only several hundred pixels to be processed (as opposed to 10^5 or 10^6 pixels); this approach is well-suited to Active Pixel cameras which permit random access of the pixel response due to selected stars. The speed and the accuracy of this approach is successfully demonstrated in comparison with the ordinary centroiding algorithms which don't use the previous image data. The predictive centroiding algorithm will be used in the GIFTS EO-3 mission in 2003. Also, the image smear problem is studied when we have high S/C angular velocity or high integration time of the camera. We Conclude image smear can present significant problems for the astigmatism based optical tagging in split field of view cameras. This problem requires further study. We show simulation results that indicate the

actual S/C angular velocity can be increase to 2 or 3 times the value of the analytical angular velocity estimate and the centroid measurement errors will be within the allowable limits.

References

[1] Mortari, D., Pollock, T.C., and Junkins, J.L. "Towards the Most Accurate Attitude determination System Using Star Trackers," Advances in the Astronautical Sciences, Vol. 99, Pt. II, pp. 839-850.

[2] Junkins, J.L., Pollock T.C., and Mortari, D. "Multiple Field of View Optical Imaging System and Method," U.S. Patent Pending No. 60/239,559, Jan, 29, 2001.

[3] Shalom, E., Alexander, J.W., and Stanton, R.H., "Acquistion and Tracking Algorithms for the ASTROS Star Tracker", Paper AAS 85-050, The Annual Rocky Mountain Guidance and Control Conference, Keystone, CO, 1985.

[4] Mortari, D. "Attitude Demonstration Using the Multiple FOVs Star Tracker StarNav III," ASI Contract NI/184/00/0. 30 September 2001. Final Report.

[5] Mortari, D., and Romoli, A. "NavStar III: A Three Fields Of View Star Tracker," 2002 IEEE Aerospace Conference, Big Sky, MT, March 9-16, 2002.

[6] Samaan, M.A., Mortari, D., and Junkins, J.L., "Recursive Mode Star Identification Algorithms", Paper AAS 01-194 Space Flight Mechanics Meeting, Santa Barbara, CA, 11-14 February, 2001.

[7] Mortari, D. "Second Estimator of the Optimal Quaternion," *Journal of Guidance, Control, and Dynamics*, Vol. 23, No. 5, Sept.-Oct. 2000, pp. 885-888.

[8] Mortari, D., and Junkins, J.L. "SP-Search Star Pattern Recognition for Multiple Fields of View Star Trackers," Paper 99-437 of the AAS/AIAA Astrodynamics Specialist Conference, Girdwood, AK, August 15-19, 1999.

[9] Mortari, D., Junkins, J.L., and Samaan, M.A. "Lost-In-Space Pyramid Algorithm for Robust Star Pattern Recognition", Paper AAS 01-004 Guidance and Control Conference, Breckenridge, Colorado, 31 Jan. - 4 Feb. 2001.

[10] Mortari, D., Bruccoleri, C., La Rosa, S., and Junkins, L.J. "CCD Data Processing Improvements," International Conference on Dynamics and Control of Systems and Structures in Space 2002, King College, Cambridge, England, July 14-18, 2002.